
DR RICHARD M LAINE (Orcid ID : 0000-0003-4939-3514)

Article type : Article

Chemical modification in and on single phase $[\text{NiO}]_{0.5}[\text{Al}_2\text{O}_3]_{0.5}$ nanopowders produces “chocolate chip-like” $\text{Ni}_x@[\text{NiO}]_{0.5-x}[\text{Al}_2\text{O}_3]_{0.5}$ nanocomposite nanopowders.

Fei Wang,^{1,2} Kai Sun,¹ Eongyu Yi,¹ Richard M. Laine *¹

¹ Department of Materials Science and Engineering, University of Michigan, Ann Arbor, MI 48109-2136

² Institute of Power Source & Ecomaterials Science, Hebei University of Technology, 300130 Tianjin, China

* E-mail: talsdad@umich.edu

Abstract

This is the author manuscript accepted for publication and has undergone full peer review but has not been through the copyediting, typesetting, pagination and proofreading process, which may lead to differences between this version and the Version of Record. Please cite this article as doi: [10.1111/JACE.16632](https://doi.org/10.1111/JACE.16632)

This article is protected by copyright. All rights reserved

Phase-pure $[\text{NiO}]_{0.5}[\text{Al}_2\text{O}_3]_{0.5}$ spinel NPs with limited aggregation were obtained via liquid-feed flame spray pyrolysis (LF-FSP) by combusting metalloorganic precursor solutions. Thereafter “chocolate chip-like” $\text{Ni}_x[\text{NiO}_{0.5-x}][\text{Al}_2\text{O}_3]_{0.5}$ nanoparticles consisting of primary $[\text{NiO}_{0.5-x}][\text{Al}_2\text{O}_3]_{0.5}$ particles with average particle sizes of 40-60 nm decorated with Ni metal particles (< 10 nm in diameter) dispersed on the surface were synthesized by heat treating the spinel NPs at 800°C/7 h in flowing 5% $\text{H}_2:\text{N}_2$ 100 mL/min in a fluidized bed reactor. The synthesized materials were characterized using TEM, XRD, FTIR and TGA/DTA. The Ni depleted areas consist primarily of $\gamma\text{-Al}_2\text{O}_3$. The Ni content (800 °C) was determined by TGA to be ≈ 11.3 wt.% based on TGA oxidation behavior. The successful synthesis of such nanocomposites with limited aggregation on a high temperature support provides a facile route to synthesize well-defined NP catalysts. This work serves as a baseline study for an accompanying paper, wherein thin, flexible, dense films made from these same NPs are used as regenerable catalysts for carbon nanotube syntheses.

Keywords: Liquid feed-flame spray pyrolysis; phase pure spinel nanopowders; nickel aluminate; nanocomposites

1. Introduction

The search for low-cost, high-performance catalysts for energy related processes continues to be a research hot spot recently as the world shifts from coal to natural gas energy feedstocks. Thus more and more emphasis has been placed on developing metal catalysts with very high and stable activity and also on exploring materials and methods of replacing precious metals i.e. Pt, Pd, Ru with less costly metals while also compensating for lower catalytic activities.¹⁻⁶ Compared with precious metals, nickel and other transition metals are relatively more abundant and following appropriate activation can offer high catalytic activity.⁷⁻¹² Equally important is the development of high activity catalysts that maintain their activity with time especially at higher processing temperatures.

In general, the high temperature stability of most metal catalysts is relatively low. It has long been recognized that deactivation pathways often involved sintering (Ostwald ripening) of metal particles on support surfaces. Likewise, the role of support materials in stabilizing catalysts is also well recognized and long studied. In particular, Al_2O_3 and SiO_2 supported nickel-based catalysts are widely used in

This article is protected by copyright. All rights reserved

industry. Such supported non-precious metal catalysts offer the advantages of low cost, wide utility, ease of recovery combined with high activity, selectivity and stability especially for reforming and hydrogenation processes.¹³⁻¹⁸

Conventional preparative methods for these kinds of catalysts typically employ various forms of solution impregnation.¹⁹⁻²² When the supported metal catalyst is prepared by impregnation, the precursor to the active metal component is affected by support surface tension, chemistries and solvation effects within the impregnation solution, ease of deposition defined by surface wetting as well as the dynamics of drying. Obviously, there are multiple variables controlling the interactions between the precursor metal salts and the support during and after impregnation that define the extent of surface coverage, potential for precursor crystallization or aggregation during deposition and activation thereafter. Thus, optimizing activity and specific active surface area can sometimes be considered an art-form rather than good science. In this paper, we describe a completely different approach that relies on synthesized high surface area NPs that can be carefully transformed to active catalytic systems without first introducing an impregnation step. In this process, active catalyst nanoparticles are proposed to be generated by chemically modifying the supporting high surface area phase. Our approach begins with the synthesis of high surface area (60 m²/g) nickel-containing spinel NPs, [NiO]_{0.5}[Al₂O₃]_{0.5}.

Spinel oxide crystal lattice ions often form with both 2⁺ and 3⁺ ions found interchangeably in both the tetrahedral and octahedral positions depending on the elements involved and leading to a wide variety of properties.²³⁻²⁶ Theoretically, transition metal aluminum spinel oxides especially nickel-containing offer considerable potential and practical applications as catalysts for such reactions as hydrocarbon cracking, methane- and methanol-steam reforming, and dehydrogenation.²⁷⁻³² Alumina supported nickel catalysts are relatively inexpensive compared to other types of catalysts. Therefore, considerable effort has been devoted to exploring and optimizing their properties.³³⁻³⁶ Perhaps most important is the fact that it is relatively difficult to obtain high surface area spinel based active catalysts due to the fact that high temperature processing is required simply to produce the spinel structure. Such high temperature processing frequently equates to extensive loss of surface area.

In the current study, the inherent thermal stability provided by a spinel phase allows generation of high surface area nanoparticles that can be reductively modified by exposure to H₂ to decorate the surface of the [NiO]_{0.5}[Al₂O₃]_{0.5} NPs with well dispersed and uniform sized catalytically active nickel metal particles. In principle, this approach may allow one to reduce side reactions caused by sintering (Ostwald ripening) of the active nickel metal particles.

Nickel aluminate spinels have been prepared via many methods including solid-state reaction, ultrasound irradiation-assisted precursor processing, sol-gel processing, and ion exchange in zeolites.³⁷⁻⁴² However, it is very difficult to prepare single-phase, nickel aluminate spinels with high surface areas and controlled stoichiometries. The as-prepared nickel aluminate spinels still suffer from serious powder agglomeration, uneven particle size distributions, and oversized particles, which affect seriously the application of nickel aluminate spinels in many fields. As a very effective method of generating a wide variety of single and mixed metal oxide NPs from metalloorganic precursors, liquid feed flame spray pyrolysis (LF-FSP) has been employed by many groups.⁴³⁻⁵⁴ Our group typically uses 1-10 wt. % ceramic yield ethanol solutions of metal carboxylates, alkoxides, beta-diketonates and/or related metalloorganic precursors to prepare a wide variety of single and mixed-metal oxide NPs that provide novel catalyst.⁵¹⁻⁵³

As practiced, these precursor solutions are aerosolized with oxygen, combusted at flame temperatures of 800-1200 °C in a 1.5 m long quartz or stainless-steel tube to produce a cloud of ions. This cloud of ions is quenched in a time frame of just a few 100 msec to temperatures of 300-400 °C. Thus, the solution and then the gas phase composition are usually retained in the resultant NPs.

The “as-shot” NPs are typically agglomerated but not aggregated, making them easy to disperse. They normally exhibit average particle sizes (APSs) of 40-100 nm equated with specific surface areas (SSAs) of 100-20 m²/g. The NPs produced can be amorphous or offer simple crystal structures (easiest to form during quenching) this includes phases not normally observed in the phase diagrams of the components as kinetic products formed during the rapid quench. In some examples, core-shell structures or even three-phase NPs form (nanostructured NPs) if all the phases are immiscible.⁵³

Early LF-FSP studies sought to develop a picture of the breadth of scope of LF-FSP for NP synthesis. We coincidentally probed NP photophysical finding that rare earth doped δ-Al₂O₃ NPs

exhibit incoherent lasing for example.⁵⁵⁻⁵⁶ As briefly noted above we also were able to demonstrate novel catalytic properties for a series of core-shell $Ce_{1-x}Zr_xO_2@δ-Al_2O_3$. Recently we reported on the utility of selected cobalt spinel NPs for the synthesis of carbon nanotubes.⁵⁷⁻⁵⁹ These results coupled with an interest in using nickel based thin films as catalysts allowed us to demonstrate the potential utility of a thin, flexible ceramic nickel aluminate as a precursor to regenerable catalysts for carbon nanotube syntheses.⁶⁰

Consequently, LF-FSP makes it possible to synthesize a wide variety of mixed-metal oxide NPs with close to atomic mixing, high purity, limited aggregation, with well controlled stoichiometries and phase compositions. LF-FSP provides a feasible way to develop novel nickel/nickel aluminate nanocomposites powders and thereafter catalysts, using nickel aluminate spinel NPs as the starting point. To our knowledge there are few related reports that have explored this approach. Furthermore, the work reported here provides a novel structure using nickel aluminate spinel NPs as the functional catalyst carrier for nickel metal, which the basic science behind our thin film CNT catalyst systems can enhance the catalytic activity along with the high added value utilization of nickel aluminate spinel NPs. Besides, nickel aluminate spinel NPs as a functional carrier can be regarded as a source of nickel metal, and the dispersibility of active nickel metal can be improved significantly.

2. Experimental

2.1. Sample preparation

Precursors. Alumatrane $Al(OCH_2CH_2)_3N$, was prepared as described elsewhere.⁵² Nickel acetate, $Ni(O_2CCH_3)_2$ was purchased from Sigma Aldrich (Milwaukee, WI) and used as received. Anhydrous ethanol fuel and solvent was purchased from Decon Labs (King of Prussia, PA).

Nanopowder synthesis. $[NiO]_{0.5}[Al_2O_3]_{0.5}$ NPs were synthesized by LF-FSP as reported previously.⁵³ Alumatrane and nickel acetate were dissolved in EtOH at the selected molar ratio to give a solution with an approximate ceramic yield of 3 wt. %. This precursor solution was aerosolized with oxygen and combusted in a chamber with methane/oxygen torches and shield O_2 .⁵³ The NPs were collected downstream in electrostatic precipitators (ESP) operated at a 10 kV direct current potential.

Fluidized bed reactor (FBR). As-prepared $[\text{NiO}]_{0.5}[\text{Al}_2\text{O}_3]_{0.5}$ NPs were placed in a quartz tube reactor and heated at selected temperatures of 500° to 900°C at 10 °C/min/7 h in 100 mL/min 5/95 $\text{H}_2:\text{N}_2$ flow Figure 1.

2.2. Materials characterization

X-ray diffraction (XRD) analyses were performed on a Rigaku Rotating Anode Goniometer (Rigaku Denki., LTD., Tokyo, Japan) with Cu $K\alpha$ radiation of 1.54 Å, a tube voltage of 40 kV and a tube current of 100 mA. Samples were placed in amorphous silica sample holders, and then scanned at a rate of 2°/min from 10° to 70° 2θ in 0.02° increments. The obtained XRD patterns were analyzed by means of Jade 2010 software (Version 1.1.5 from Mater. Data, Inc.). Peak positions and relative intensities were identified in comparison with the reference powder diffraction data (JCPDS) files.

TEM studies of sample microstructures were run on a JEOL 3100R05 Double Cs Corrected TEM/STEM operated at an acceleration voltage of 300 kV with the Gatan Ultrascan 1000 CCD TV camera for high resolution imaging, and a JEOL 2100F Probe-corrected Electron Microscope at an acceleration voltage of 200 kV with an EDAX 60 mm² SDD detector (active area = 60 mm²) capable of detecting elements with $Z > 5$.

Thermal gravimetric analysis (TGA) and differential thermal analysis (DTA) were performed on a SDT Q600 simultaneous TGA-DTA instrument. About 20 mg of powder samples were pressed to a small pellet and loaded in an alumina pan, using an empty pan as reference. Then the samples were heated from room temperature to 1000°C at 10 °C min⁻¹ in 60 mL/min of flowing air.

Fourier transform infrared spectra (FTIR) were obtained on a NICOLET 6700 using KBr discs to monitor changes in atomic bonding during chemical modification. Optical grade KBr, 400 mg (International Crystal Laboratories, Garfield, NJ), was ground using an alumina mortar and pestle, and 5 mg of sample was added and ground together. The ground samples were loaded in the FTIR sample holder, and loaded into instrument. Then the sample chamber was purged with N_2 (10-15 min) to remove atmospheric CO_2 . Each spectrum is continuous in the range 4000-400 cm^{-1} with a scan resolution of 4 cm^{-1} with an average of 130 scans, using OMNIC software package.

3. Results and discussion

This article is protected by copyright. All rights reserved

The overall objective of the work reported here is to demonstrate that careful treatment of single phase but mixed-metal nanoparticles with a reducing agent, can selectively reduce one component of the single phase to generate phase separation while still maintaining the nanoscale properties of the individual nanopowders. Such a process was envisioned to produce “chocolate chip” like nanocomposites with the catalytically active species decorating the partially reduced substrate, as suggested in Figure 2.

We recently demonstrated this same approach wherein treatment of nearly single phase $(\text{TiO}_2)_{0.43}(\text{Al}_2\text{O}_3)_{0.57}$ nanopowders with NH_3 reduces the TiO_x component likely by the same pathway as suggested in Figure 2 but with segregation to form more stable $\text{TiN@Al}_2\text{O}_3$ core shell nanocomposites.⁵⁹ We also suspect that a similar process occurs in the transformation of $[\text{CoO}]_{0.x}[\text{Al}_2\text{O}_3]_{1-x}$ where $x = 0.25$ or 0.50 to active catalyst species in the gas phase synthesis of carbon nanotubes (CNTs) from such nanopowders under reducing conditions.⁵⁸

In the current studies, we attempt to carefully define the phase separation process for the title materials to establish the basis for creating Ni nanoparticle catalysts for CNT syntheses where the spinel nanopowders are first processed into dense flexible films. The studies reported here provide an understanding of the processes that lead to catalyst particle formation in a recently published work.⁶⁰

3.1. Effect of reduction process on the crystal structure of as prepared nanocomposites

Figure 2 provides XRDs of as-prepared $[\text{NiO}]_{0.5}[\text{Al}_2\text{O}_3]_{0.5}$ NPs (control) and derived nanocomposites reduced for 7 h at different temperatures in flowing (100 mL/min) 5/95 $\text{H}_2:\text{N}_2$, in the course of optimizing the reduction process.

Figure 3 shows XRDs from both the as-produced $[\text{NiO}]_{0.5}[\text{Al}_2\text{O}_3]_{0.5}$ NPs (control) and reduced samples. The $[\text{NiO}]_{0.5}[\text{Al}_2\text{O}_3]_{0.5}$ spinel phase is the only phase present at reduction temperatures below 700 °C. Above 700 °C, diffraction peaks for cubic nickel (marked as c) appear with very weak intensities. At temperature 800°C, several obvious peaks for metallic nickel can be observed. Coincidentally, both nickel spinel (marked as a) and Al_2O_3 (marked as b) diffraction peaks are observed. In contrast, at 900 °C the XRD pattern shows primarily metallic Ni and $\gamma\text{-Al}_2\text{O}_3$. Based on

this set of studies, 800 °C was selected as the optimal temperature for producing high surface area, Ni on Al₂O₃ NPs to optimize chocolate chip-like nanocomposite processing.

3.2. Fourier transform infrared spectroscopy (FT-IR)

To further confirm the formation of Al₂O₃ in the above nanocomposites, the chemical characteristics of the different nanocomposites samples were monitored by FT-IR as shown in Figure 4.

Figure 4 shows that a small new peak appearing around 825 cm⁻¹ at a reduction temperature of ≥ 750 °C, which becomes more obvious at 800 °C. New peaks appearing near 600 and 800 cm⁻¹ correspond to octahedrally and tetrahedrally coordinated νAl-O coincident with nickel generation,^{45,61,62} as expected from the XRD results. The new peaks become more obvious as temperatures increase to 900°C as metallic Ni is produced which must coincidentally generate Al₂O₃.

3.3. Thermal gravimetric analysis (TGA) and differential thermal analysis (DTA)

To obtain Ni metal contents in the above nanocomposites, TGA analyses were run of the as-produced powders and of the 800 °C reduced powders per Figures 5a and b. In Figure 5a, there is no obvious mass gain whereas in 5b, an obvious mass gain appears between 200° and 400 °C. The mass gain is directly proportional to the formation of NiO from Ni, and the Ni metal contents can be estimated to be about 11 wt %.

3.4. Microstructures of nanocomposites

Figures 6 and 7 provide STEM bright-field (BF) image and element mapping results. Figure 6 shows typical particle distributions and morphologies characteristic of 800 °C reduced NPs. All NPs exhibit similar spherical and homogeneous morphologies, mostly smaller than 60 nm. The many dark, small spots evenly distributed on the surface of the NPs likely correspond to Ni metal particles. In Figure 7, element mapping of O, Al and Ni are displayed in red, yellow and blue, respectively. As is evident both O and Al are uniformly distributed. More Ni can be observed coincident with the small dark spots distributed on the NP surfaces as anticipated.

Figure 8 HRTEM provides two more complete assessments of the [Ni]_x[NiO]_{0.5-x}[Al₂O₃]_{0.5} nanocomposite morphology, confirming their chocolate chip-like microstructure. Besides, Figure 8 shows two representative nickel metal particles < 10 nm in diameter dispersed evenly on the surface of

[NiO]_{0.5-x}[Al₂O₃]_{0.5} spinel NPs, confirming the formation of a chocolate chip-like nanocomposite. The same HRTEM images show Al₂O₃ formed at the edge of nickel particle, consistent with the XRD and FTIR results.

Conclusions

In this work, we describe a method of transforming a single phase nanopowder into a nanocomposite nanopowder without loss of nanoscale properties. This work sets the tone for the development of a series of catalysts with high surface area and presumably high activity on high surface area substrates very difficult to generate via any other process we are aware. This work also provides the baseline science elucidating the reduction process that occurs in thin films of similar materials used as regenerable nanocomposite catalysts for carbon nanotube syntheses.⁶⁰ In this process, careful reduction of the nickel component in [NiO]_{0.5}[Al₂O₃]_{0.5} spinel nanopowders in flowing 5/95 H₂:N₂ leads to local reduction of some portion of the NiO likely near the surface of the original nanopowders to produce a spinel nanopowder decorated with Ni metal nanoparticles. The process can be considered as an approach to making a wide variety of catalytic “chocolate chip-like” nanocomposites.

The Ni metal particle sizes appear to be typically smaller than 10 nm and evenly distributed on the surface of [NiO]_{0.5}[Al₂O₃]_{0.5} spinel nanopowders. Coincidentally, γ -Al₂O₃ forms at the edge of nickel particles. The limited aggregation with good stoichiometric control offers the potential to develop a number of such nanocomposite materials for catalytic applications for example. Finally, these results serve as baseline data for the catalytic reduction of [NiO]_{0.5}[Al₂O₃]_{0.5} derived thin films that can be used to catalytically generate carbon nanotubes and whose catalytic reactivity can be regenerated.⁶⁰ Indeed we suspect it also occurs in the gas phase process wherein [CoO]_x[Al₂O₃]_{1-x} nanoparticles are reduced in flowing hydrogen and thereafter used to catalyze formation of carbon nanotubes as demonstrated in Figure 4 of ref. 58.

Acknowledgments

We are grateful for the financial support of this work by NSF through DMR-0723032. Fei Wang would also like to thank the financial support by China Scholarship Council. JEOL JEM-2100F and the

JEOL JEM- 3100R05 aberration-corrected TEMs were obtained using support of the University of Michigan College of Engineering and NSF grant #DMR-0723032

References

1. Kamiguchi S, Nagashima S, Chihara T. Application of solid-state early-transition metal clusters as catalysts. *Tetrahedron Lett.* 2018; 59(14):1337-1342.
2. Suo H, Solan GA, Ma Y, Sun W. Developments in compartmentalized bimetallic transition metal ethylene polymerization catalysts. *Coord Chem Rev.* 2018; 372:101-116.
3. Takenaka S, Kaji R, Sugiyama K, Ida R. Preparation of composite catalysts composed of Pt nanoparticles and metal oxide nanosheets: Preferential formation of Pt/metal oxide interfaces. *Appl Catal, A.* 2018; 566:52-59.
4. Hita I, Deuss P, Bonura G, Frusteri F, Heeres H. Biobased chemicals from the catalytic depolymerization of Kraft lignin using supported noble metal-based catalysts. *Fuel Process Technol.* 2018; 179:143-153.
5. Almutairi S, Kozhevnikova E, Kozhevnikov I. Ketonisation of acetic acid on metal oxides: Catalyst activity, stability and mechanistic insights. *Appl Catal, A.* 2018; 565:135-145.
6. Schmal M, Toniolo FS, Kozonoe CE. Perspective of catalysts for (Tri) reforming of natural gas and flue gas rich in CO₂. *Appl Catal, A.* 2018; 568:23-42.
7. Huang H, Lu H, Zhan Y, Liu G, Feng Q, Huang H, et al. VUV photo-oxidation of gaseous benzene combined with ozone-assisted catalytic oxidation: Effect on transition metal catalyst. *Appl Surf Sci.* 2017; 391:662-667.
8. Min JE, Lee YJ, Park HG, Zhang C, Jun KW. Carbon dioxide reforming of methane on Ni-MgO-Al₂O₃ catalysts prepared by sol-gel method: Effects of Mg/Al ratios. *J Ind Eng Chem.* 2015; 26:375-383.
9. Shin D, An X, Choun M, Lee J. Effect of transition metal induced pore structure on oxygen reduction reaction of electrospun fibrous carbon. *Catal Today.* 2016; 260:82-88.
10. Salam MA, Abdullah B. Catalysis mechanism of Pd-promoted γ -alumina in the thermal decomposition of methane to hydrogen: A density functional theory study. *Mater Chem Phys.* 2017; 188:18-23.
11. Wang F, Xie Z, Liang J, Fang B, Piao Y, Hao M, et al. Tourmaline-modified FeMnTiO_x catalysts for improved low-temperature NH₃-SCR performance. *Environ Sci Technol.* 2019; 00:1-8. <http://dx.doi.org/10.1021/acs.est.9b02620>.
12. Keum C, Kim MC, Lee SY. Effects of transition metal ions on the catalytic activity of carbonic anhydrase

-
- mimics. *J Mol Catal A: Chem.* 2015; 408:69-74.
13. Manukyan KV, Cross AJ, Yeghishyan AV, Rouvimov S, Miller JJ, Mukasyan AS, et al. Highly stable Ni–Al₂O₃ catalyst prepared from a Ni–Al layered double hydroxide for ethanol decomposition toward hydrogen. *Appl Catal, A.* 2015; 508:37-44.
 14. Salazar AFS, Chave T, Ayrat A, Nikitenko SI, Hulea V, Kooyman PJ, et al. Engineering of silica-supported platinum catalysts with hierarchical porosity combining latex synthesis, sonochemistry and sol-gel process—I. Material preparation. *Microporous Mesoporous Mater.* 2016; 234:207-214.
 15. Jiménez-González C, Boukha Z, Rivas BD, González-Velasco JR, Gutiérrez-Ortiz JI, López-Fonseca R. Behavior of coprecipitated NiAl₂O₄/Al₂O₃ catalysts for low-temperature methane steam reforming. *Energy Fuels.* 2014; 28:7109–7121.
 16. Banerjee AM, Pai MR, Tewari R, Raje N, Tripathi AK, Bharadwaj SR, et al. A comprehensive study on Pt/Al₂O₃ granular catalyst used for sulfuric acid decomposition step in sulfur–iodine thermochemical cycle: Changes in catalyst structure, morphology and metal-support interaction. *Appl Catal, B.* 2015; 162:327-337.
 17. Zhou L, Li L, Wei N, Li J, Takanabe K, Basset JM. Effect of NiAl₂O₄ formation on Ni/Al₂O₃ stability during dry reforming of methane. *ChemCatChem.* 2015; 7(16):2406-2406.
 18. Yuan P, Cui C, Han W, Bao X. The preparation of Mo/ γ -Al₂O₃ catalysts with controllable size and morphology via adjusting the metal-support interaction and their hydrodesulfurization performance. *Appl Catal, A.* 2016; 524:115-125.
 19. Tao M, Meng X, Lv Y, Bian Z, Xin Z. Effect of impregnation solvent on Ni dispersion and catalytic properties of Ni/SBA-15 for CO methanation reaction. *Fuel.* 2016; 165(4):289-297.
 20. Wen X, Li R, Yang Y, Chen J, Zhang F. An egg-shell type Ni/Al₂O₃ catalyst derived from layered double hydroxides precursor for selective hydrogenation of pyrolysis gasoline. *Appl Catal, A.* 2013; 468:204-215.
 21. Li B, Qian X, Wang X. Oxidative CO₂ reforming of methane over stable and active nickel-based catalysts modified with organic agents. *Int J Hydrogen Energy.* 2015; 40(25):8081-8092.
 22. Danilova MM, Fedorova ZA, Zaikovskii VI, Porsin AV, Kirillov VA, Krieger TA. Porous nickel-based catalysts for combined steam and carbon dioxide reforming of methane. *Appl Catal, B.* 2014; 147(7):858-863.
 23. Takahashi S, Kan A, Ogawa H. Microwave dielectric properties and crystal structures of spinel-structured MgAl₂O₄ ceramics synthesized by a molten-salt method. *J Eur Ceram Soc.* 2017; 37(3):1001-1006.

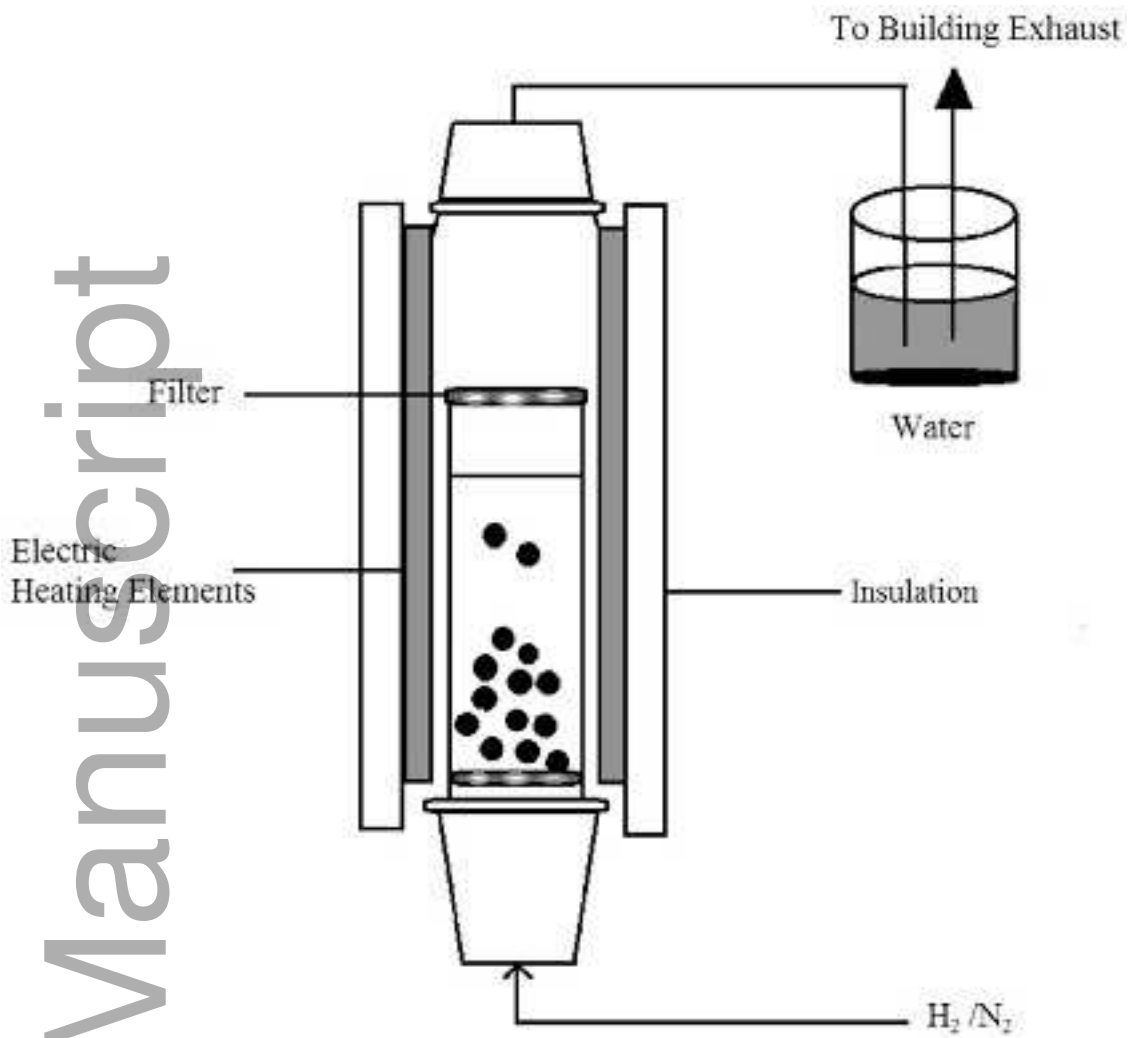
-
24. Li D, Lu M, Cai Y, Cao Y, Zhan Y, Jiang L. Synthesis of high surface area MgAl₂O₄ spinel as catalyst support via layered double hydroxides-containing precursor. *Appl Clay Sci.* 2016; 132:243-250.
 25. Gupta SK, Pathak N, Ghosh PS, Kadam RM. On the photophysics and speciation of actinide ion in MgAl₂O₄ spinel using photoluminescence spectroscopy and first principle calculation: A case study with uranium. *J Alloys Compd.* 2017; 695:337-343.
 26. Samkaria R, Sharma V. Effect of rare earth yttrium substitution on the structural, dielectric and electrical properties of nanosized nickel aluminate. *Mater Sci Eng, B.* 2013; 178(20):1410-1415.
 27. Santillan-Jimenez E, Loe R, Garrett M, Morgan T, Crocker M. Effect of Cu promotion on cracking and methanation during the Ni-catalyzed deoxygenation of waste lipids and hemp seed oil to fuel-like hydrocarbons. *Catal Today.* 2018; 302:261-271.
 28. He L, Hui H, Li S, Lin W. Production of light aromatic hydrocarbons by catalytic cracking of coal pyrolysis vapors over natural iron ores. *Fuel.* 2018; 216:227-232.
 29. Thattarathody R, Sheintuch M. Kinetics and dynamics of methanol steam reforming on CuO/ZnO/alumina catalyst. *Appl Catal, A.* 2017; 540:47-56.
 30. Bagherzadeh SB, Haghighi M. Plasma-enhanced comparative hydrothermal and coprecipitation preparation of CuO/ZnO/Al₂O₃ nanocatalyst used in hydrogen production via methanol steam reforming. *Energy Convers Manage.* 2017; 142:452-465.
 31. Correa A, Cascella M, Scotti N, Zaccheria F, Ravasio N, Psaro R. Mechanistic insights into formic acid dehydrogenation promoted by Cu-amino based systems. *Inorg Chim Acta.* 2018; 470:290-294.
 32. Kalenchuk AN, Bogdan VI, Dunaev SF, Kustov LM. Dehydrogenation of polycyclic naphthenes on a Pt/C catalyst for hydrogen storage in liquid organic hydrogen carriers. *Fuel Process Technol.* 2018; 169:94-100.
 33. Karaman BP, Cakiryilmaz N, Arbag H, Oktar N, Dogu G, Dogu T. Performance comparison of mesoporous alumina supported Cu & Ni based catalysts in acetic acid reforming. *Int J Hydrogen Energy.* 2017; 42(42):26257-26269.
 34. Papageridis KN, Siakavelas G, Charisiou ND, Avraam DG, Tzounis L, Kousi K, et al. Comparative study of Ni, Co, Cu supported on γ -alumina catalysts for hydrogen production via the glycerol steam reforming reaction. *Fuel Process Technol.* 2016; 152:156-175.
 35. Kim D, Jeon J, Lee W, Lee J, Ha KS. Effective suppression of deactivation by utilizing Ni-doped ordered

-
- mesoporous alumina-supported catalysts for the production of hydrogen and CO gas mixture from methane. *Int J Hydrogen Energy*. 2017; 42(39):24744-24756.
36. Braidy N, Bastien S, Blanchard J, Fauteux-Lefebvre C, Achouri IE, Abatzoglou N. Activation mechanism and microstructural evolution of a YSZ/Ni-alumina catalyst for dry reforming of methane *Catal Today*. 2017; 291:99-105.
 37. Jiménez-González C, Boukha Z, Rivas BD, González-Velasco JR, Gutiérrez-Ortiz JI, López-Fonseca R. Behaviour of nickel–alumina spinel (NiAl₂O₄) catalysts for isooctane steam reforming. *Int J Hydrogen Energy*. 2015; 40(15):5281-5288.
 38. Shamskar FR, Meshkani F, Rezaei M. Ultrasound assisted co-precipitation synthesis and catalytic performance of mesoporous nanocrystalline NiO-Al₂O₃ powders. *Ultrason Sonochem*. 2017; 34:436-447.
 39. Kumar JP, Prasad GK, Allen JA, Ramacharyulu PVRK, Kadirvelu K, Singh B. Synthesis of mesoporous metal aluminate nanoparticles and studies on the decontamination of sulfur mustard. *J Alloys Compd*. 2016; 662:44-53.
 40. Neto ASB, Oliveira AC, Filho JM, Amadeo N, Dieuzeide ML, Sousa FFD, et al. Characterizations of nanostructured nickel aluminates as catalysts for conversion of glycerol: Influence of the preparation methods. *Adv Powder Technol*. 2017; 28(1):131-138.
 41. Achouri IE, Abatzoglou N, Fauteux-Lefebvre C, Braidy N. Diesel steam reforming: Comparison of two nickel aluminate catalysts prepared by wet-impregnation and co-precipitation. *Catal Today*. 2013; 207:13-20.
 42. Nieva MA, Villaverde MM, Monzón A, Garetto TF, Marchi AJ. Steam-methane reforming at low temperature on nickel-based catalysts. *Chem Eng J*. 2014; 235:158-166.
 43. Yi JH, Kim JH, Koo HY, You NK, Kang YC, Lee JH. Nanosized LiMn₂O₄ powders prepared by flame spray pyrolysis from aqueous solution. *J Power Sources*. 2011; 196(5):2858-2862.
 44. Demirci S, Öztürk B, Yildirim S, Bakal F, Erol M, Sancakoğlu O, et al. Synthesis and comparison of the photocatalytic activities of flame spray pyrolysis and sol–gel derived magnesium oxide nano-scale particles. *Mater Sci Semicond Process*. 2015; 34:154-161.
 45. Kim JH, Hong YJ, Park BK, Kang YC. Nano-sized LiNi_{0.5}Mn_{1.5}O₄ cathode powders with good electrochemical properties prepared by high temperature flame spray pyrolysis. *J Ind Eng Chem*. 2013; 19(4):1204-1208.
 46. Kruis FE, Fissan H, Peled A. Synthesis of nanoparticles in the gas phase for electronic, optical and magnetic applications—a review. *J Aerosol Sci*. 1998; 29(5-6):511-535.

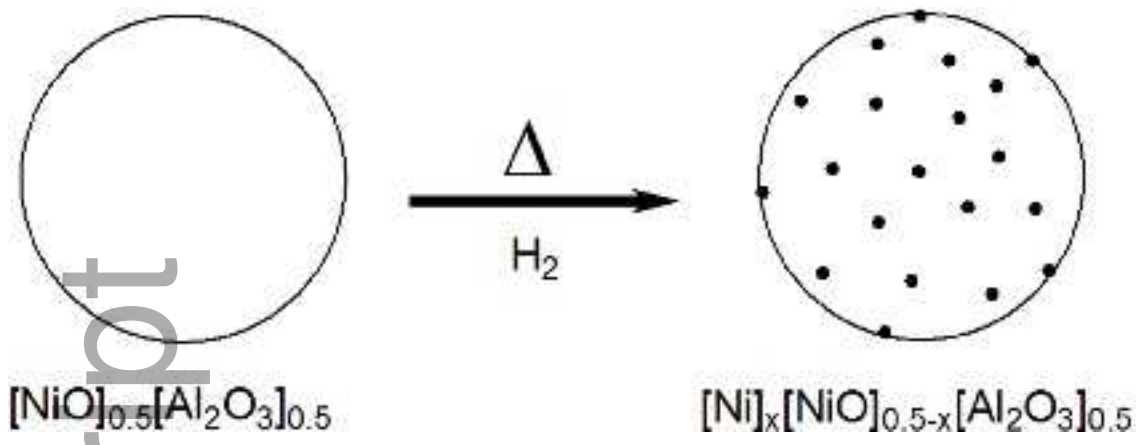
-
47. Schimmoeller B, Schulz H, Ritter A, Reitzmann A, Kraushaar-Czarnetzki B, Baiker A, et al. Structure of flame-made vanadia/titania and catalytic behavior in the partial oxidation of o-xylene. *J Catal.* 2008; 256(1):74-83.
 48. Wagner N, Svensson AM, Vullum-Bruer F. Liquid-feed flame spray pyrolysis as alternative synthesis for electrochemically active nano-sized $\text{Li}_2\text{MnSiO}_4$. *Transl Mater Res.* 2016; 3(2):025001.
 49. Suffner J, Wang D, Kübel C, Hahn H. Metastable phase formation during flame spray pyrolysis of $\text{ZrO}(\text{YO})\text{-AlO}$ nanoparticles. *Scr Mater.* 2011; 64(8):781-784.
 50. Hinklin T, Toury B, Gervais C, Babonneau F, Gislason J, Morton R, et al. Liquid-feed flame spray pyrolysis of metalloorganic and inorganic alumina sources in the production of nanoalumina powders. *Chem Mater.* 2004; 16(1):21-30.
 51. Laine RM, Bickmore CR, Treadwell DR, Waldner KF. Ultrafine metal oxide powders by flame spray pyrolysis. U.S. Patent 5958361. 1999 Sep. 28.
 52. Baranwal R, Villar M, Garcia R, Laine R. Synthesis, characterization, and sintering behavior of nano-mullite powder and powder compacts. *J Am Ceram Soc.* 2001; 84(5):951-61.
 53. Jose AA, Julien M, Patrick S, Haiping S, Xiaoqing Q. P, Richard M. L. Liquid-feed flame spray pyrolysis as a method of producing mixed-metal oxide nanopowders of potential interest as catalytic materials. nanopowders along the $\text{NiO-Al}_2\text{O}_3$ tie line including $(\text{NiO})_{0.22}(\text{Al}_2\text{O}_3)_{0.78}$, a new inverse spinel composition. *Chem. Mater.* 2006; 18(9):731-739.
 54. Taylor NJ, Stangeland-Molo S, Laine RM. Bottom-up vs reactive sintering of $\text{Al}_2\text{O}_3\text{-YAG-YSZ}$ composites via one or three-phase nanoparticles (NPs). Bottom-up processing wins this time. *J Am Ceram Soc.* 2017; 100(6):2429-2438.
 55. Li B, Williams G, Rand SC, Hinklin T, Laine RM. Continuous-wave ultraviolet laser action in strongly scattering Nd-doped alumina. *Opt Lett.* 2002; 27(6):394-396.
 56. Williams GR, Bayram SB, Rand SC, Hinklin T, Laine RM. Laser action in strongly scattering rare-earth-metal-doped dielectric nanophosphors. *Phys Rev A.* 2001; 65(1):337-339.
 57. Weidenhof B, Reiser M, Stöwe K, Maier WF, Kim M, Azurdia J, et al. High-throughput screening of nanoparticle catalysts made by flame spray pyrolysis as hydrocarbon/NO oxidation catalysts. *J Am Chem Soc.* 2009; 131(26):9207-9219.

-
58. Shirae H, Hasegawa K, Sugime H, Yi E, Laine RM, Noda S. Catalyst nucleation and carbon nanotube growth from flame-synthesized Co-Al-O nanopowders at ten-second time scale. *Carbon*. 2017; 114:31-38.
59. You F, Sun K, Yi E, Nakatani E, Umehara N, Laine RM. Chemical modification at and within nanopowders: Synthesis of core-shell $\text{Al}_2\text{O}_3@\text{TiON}$ nanopowders via nitriding nano- $(\text{TiO}_2)_{0.43}(\text{Al}_2\text{O}_3)_{0.57}$ powders in NH_3 . *J Am Ceram Soc*. 2018; 101(4):1441-1452.
60. Liang B, Yi E, Sato T, Noda S, Jia D, Zhou Y, et al. Flame synthesized $[\text{NiO}]_{0.25}[\text{Al}_2\text{O}_3]_{0.75}$ and $[\text{NiO}]_{0.50}[\text{Al}_2\text{O}_3]_{0.50}$ nanopowders (NPs) provide thin, dense, flexible $\text{NiAl}_2\text{O}_4\text{-Al}_2\text{O}_3$ and $\text{Ni-Al}_2\text{O}_3$ nanocomposite catalytic films. Regeneration of a heterogeneous catalyst by oxidative re-adsorption into a heterogeneous substrate is demonstrated for carbon nanotube syntheses. Submitted for publication.
61. Taylor NJ, Pottebaum AJ, Uz V, Laine RM. The bottom up approach is not always the best processing method: dense $\alpha\text{-Al}_2\text{O}_3/\text{NiAl}_2\text{O}_4$ composites. *Adv Funct Mater*. 2014; 24(22):3392-3398.
62. Gullapelli S, Scurrrell MS, Valluri DK. Photocatalytic H_2 production from glycerol–water mixtures over $\text{Ni}/\gamma\text{-Al}_2\text{O}_3$ and TiO_2 composite systems. *Int J Hydrogen Energy*. 2017; 42(22):15031-15043.

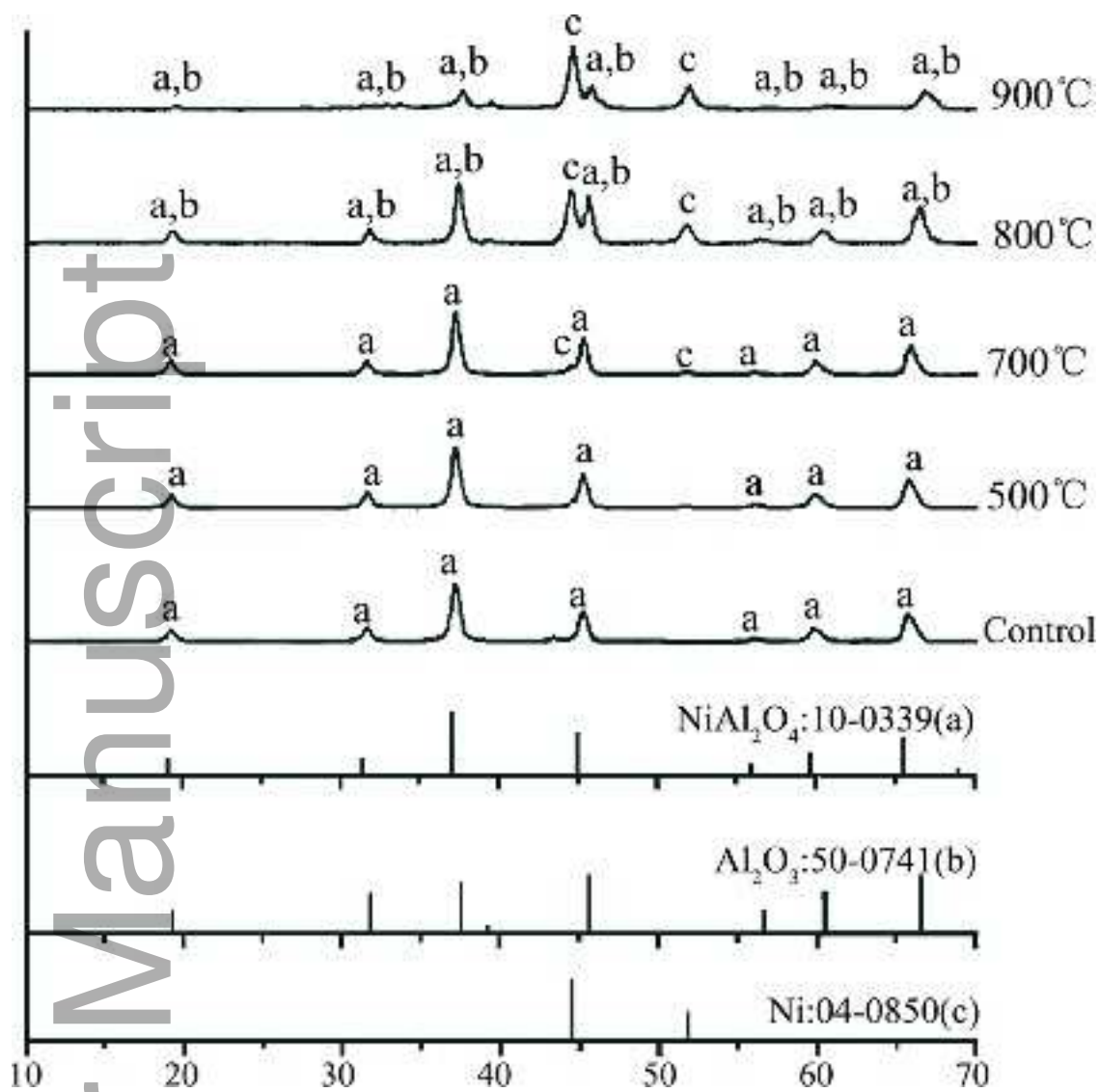
Author Manuscript



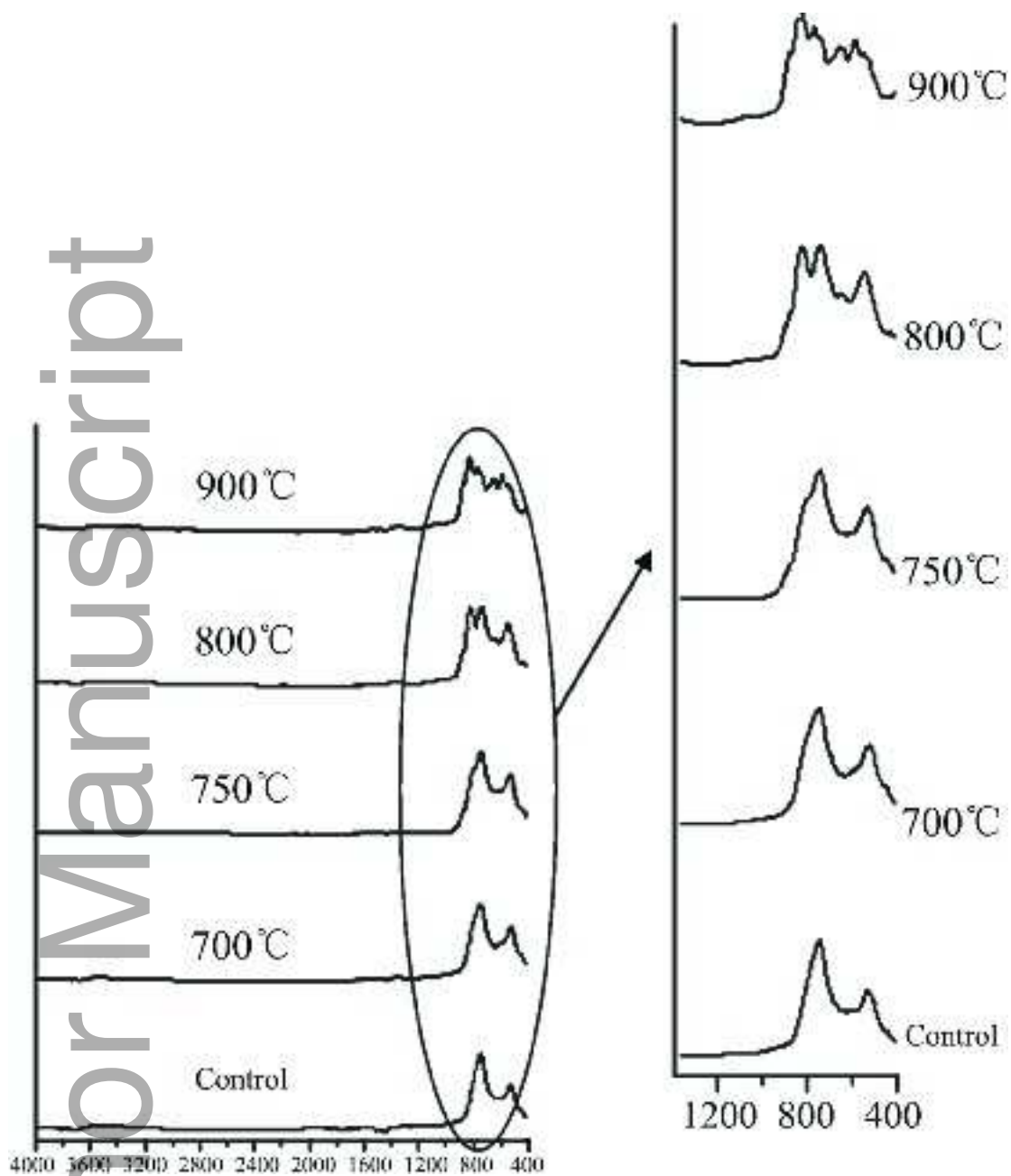
jace_16632_f1.tif



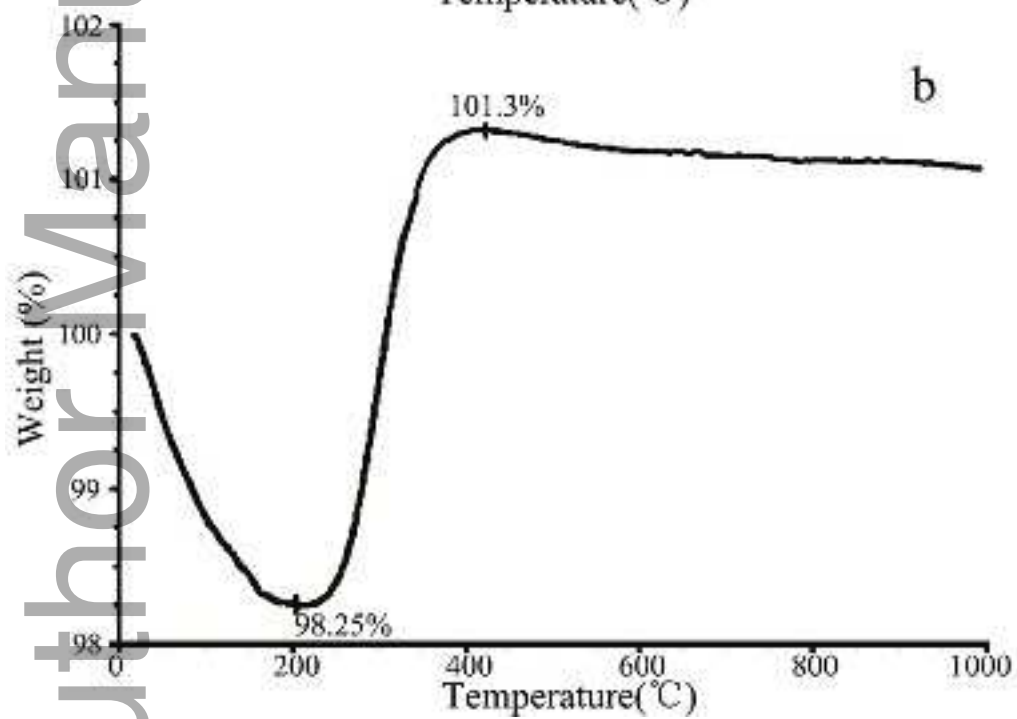
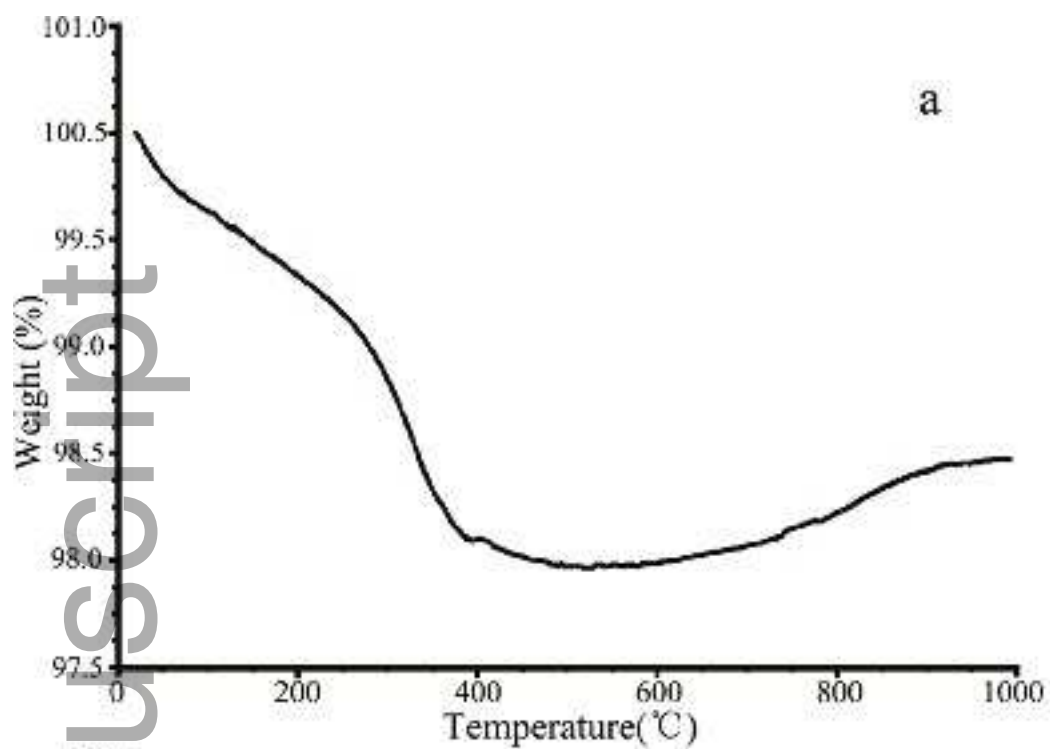
jace_16632_f2.tif



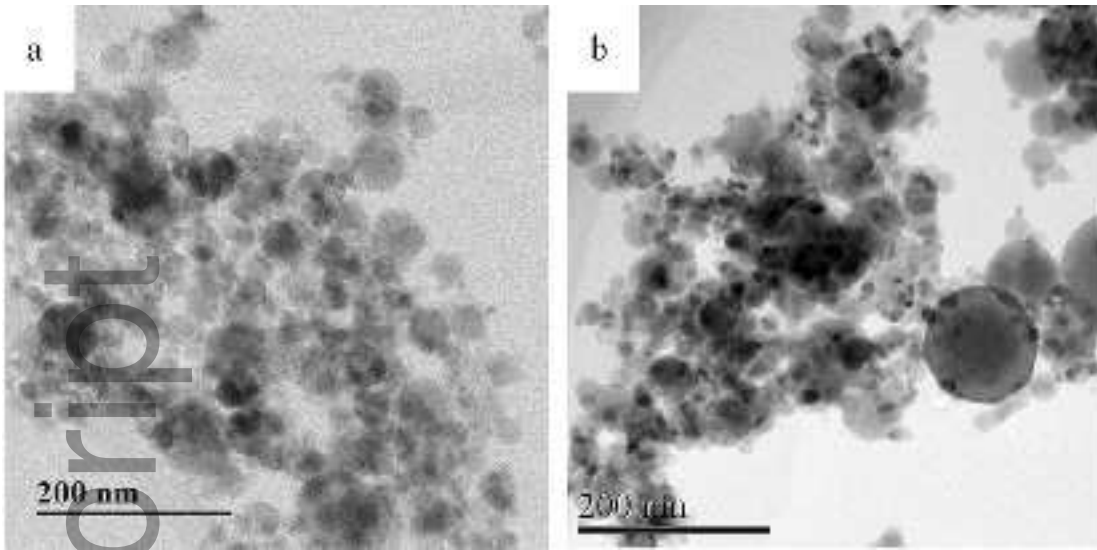
jace_16632_f3.tif



jace_16632_f4.tif

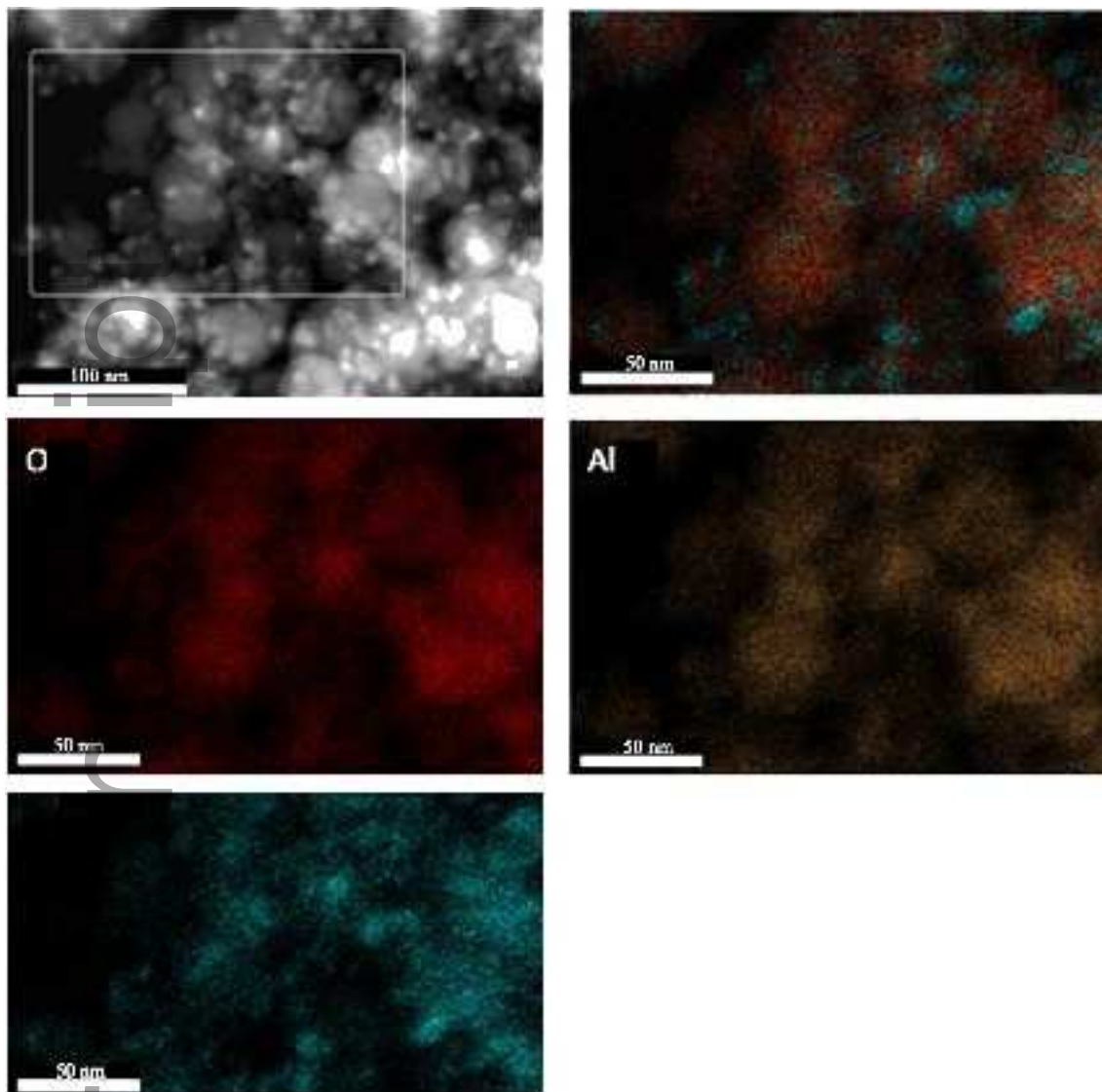


jace_16632_f5.tif

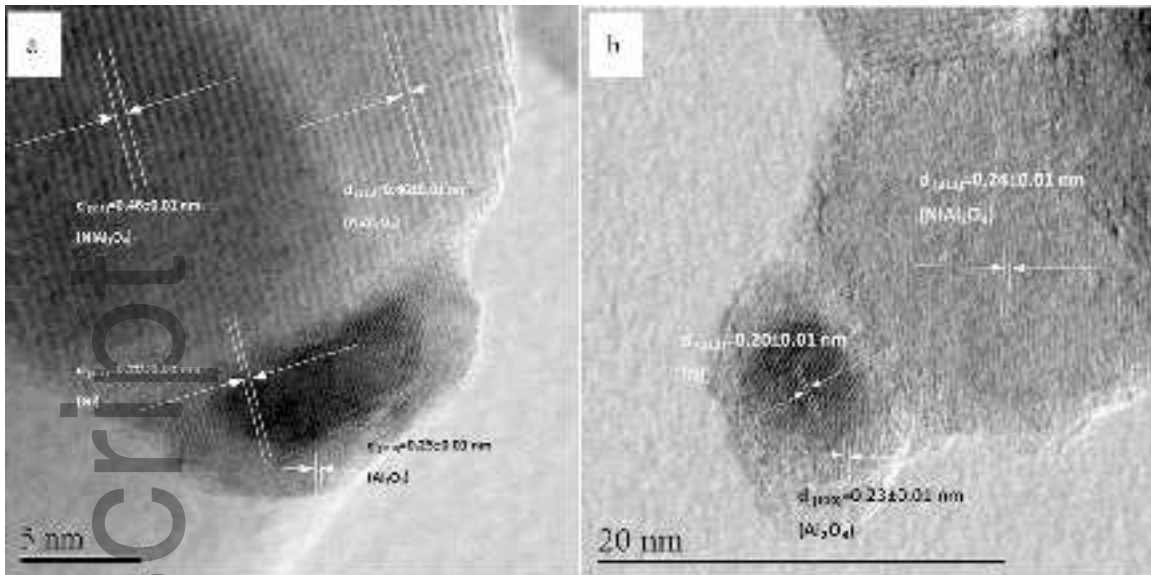


jace_16632_f6.tif

Author Manuscript



jace_16632_f7.tif



jace_16632_f8.tif